JAERI-M
9789

MAGNETIC STRUCTURE OF POLOIDAL DIVERTOR CONFIGURATION WITH NON-AXISYMMETRIC PERTURBED FIELD IN JT-60

November 1981

Hidetoshi YOSHIDA, Hiroshi KISHIMOTO, Shin YAMAMOTO
Seio SENGOKU, Masafumi AZUMI, Tomonori TAKIZUKA
Hiromasa NINOMIYA and Sanae TAMURA

日 本 原 子 力 研 究 所
Japan Atomic Energy Research Institute

JAERI-M 9789

Magnetic Structure of Poloidal Divertor Configuration with Non-Axisymmetric Perturbed Field in JT-60

Hidetoshi YOSHIDA, Hiroshi KISHIMOTO, Shin YAMAMOTO[+]
Seio SENGOKU[+], Masafumi AZUMI[+], Tomonori TAKIZUKA[+]
Hiromasa NINOMIYA and Sanae TAMURA

Division of Large Tokamak Development,
Tokai Research Establishment, JAERI

(Received October 20, 1981)

Magnetic structure of a divertor configuration in JT-60 is numerically investigated under the influence of non-axisymmetric magnetic perturbations: toroidal ripple field and error field due to mechanical tolerance of poloidal field coils. The possibilities are presented that ergodic layer formed near a separatrix, due to the magnetic perturbations, enhances a spread of a scrape-off layer and that it allows particles to escape from a boundary plasma along field lines of force.

Keywords: JT-60, Poloidal Divertor, Ergodic Layer, Scrape-off Layer, Magnetic Island, Magnetic Limiter, Toroidal Ripple Field, Separatrix, Non-Axisymmetric Magnetic Perturbation, X Point.

+) Division of Thermonuclear Fusion Research, Tokai Research Establishment, JAERI

JT－60における非軸対称揺動磁場の影響下でのポロイダルダイバータ配位の磁気構造

日本原子力研究所東海研究所大型トカマク開発部
吉田英俊・岸本　浩・山本　新[+]・仙石盛夫[+]
安積正史[+]・滝塚知典[+]・二宮博正・田村早苗

（1981年10月20日受理）

非軸対称な磁気揺動（トロイダルリップル磁場やポロイダル磁場コイルの据付誤差によるエラー磁場）の影響下でのJT－60のダイバータ配位時の磁気構造を数値的に検討した。磁気揺動によってセパラトリックス近傍の磁気面は破壊されエルゴディック層が形成される。エルゴディック層はスクレープオフ層を拡げるとともに，境界プラズマから粒子を磁力線に沿って流出させる可能性がある。

+）核融合研究部

Contents

目　　次

1. Introduction

A poloidal magnetic divertor has been noted as an attractive method for impurity control in a tokamak.[1] The magnetic structure near a separatrix magnetic surface is important to understand the property of a poloidal divertor. In an axisymmetric divertor, the separatrix surface is the boundary between a confined region and a scrape-off layer (a divertor region). There exists, however, the non-axisymmetric magnetic field in an actual tokamak which influences the ideal divertor configuration, especially near the separatrix magnetic surface.

A magnetic perturbation with angular dependence of $\exp[i(m\theta-n\phi)]$ produces a chain of magnetic islands on the rational surface with the tokamak safety factor $q = m/n$. The magnetic perturbations in an actual tokamak have many harmonics, and many rational surfaces are closely distributed near the separatrix. Thus the adjacent island chains will easily overlap with each other near the separatrix. Such an overlapping results in the destruction of the magnetic surfaces and the formation of "ergodic layer" where the field lines behave irregularly.[2-4]

For the divertor to operate effectively, it must be avoided that the field lines in the scrape-off layer strike the first wall before their reaching the neutralizer plate. This problem occurs particularly when the clearance between the separatrix and the first wall is as narrow as the scrape-off layer width. Even in the case with a relatively wide clearance, the ergodic layer produced near the separatrix can broaden the scrape-off layer and may deteriorate the divertor function of impurity exhaust.

The ergodic layer also affects plasma transport in the scrape-off layer.[5] In DIVA experiment, particle loss mechanism was accounted for the existence of the ergodic layer.[6] From these points of view, several works have been done theoretically[7,8] and numerically.[6,9,10] Especially in a large divertor tokamak with a long pulse, e.g. JT-60[11], it is very important to understand the actual magnetic structure near the separatrix.

In this paper, the magnetic structure near the separatrix in JT-60 is investigated with presumed perturbed fields: the toroidal ripple field with a high toroidal mode number and the error field due to the mechanical tolerance of the poloidal field coils with a low one.

Section 2 presents the unperturbed magnetic structure of the divertor configuration. The destruction of magnetic surfaces caused by the toroidal ripple field is examined in §3. The perturbed magnetic structure produced by the error field due to the misalignment of the poloidal field coils is investigated in §4. The results obtained in the present calculations are discussed in the final section.

2. Divertor Configuration

Equations of the magnetic field lines of force are given by

$$\frac{dR}{B_R} = \frac{Rd\phi}{B_\phi} = \frac{dz}{B_z} \quad .$$

Here, R, ϕ and z are cylindrical coordinates, B_ϕ the toroidal magnetic field, and B_R and B_z the poloidal ones, respectively. The poloidal field in a Tokamak is produced by the plasma current as well as by the external coil currents for the plasma equilibrium and shaping.

The flux function at an observing point (R, z) produced by a unit ring current centered at $z = \zeta$ with a ring radius ρ is given by

$$\Psi(R,z;\rho,\zeta) = \frac{\mu_0}{\pi\kappa}\sqrt{R\rho}\,\{(1 - \frac{\kappa^2}{2})K(\kappa) - E(\kappa)\} \ ,$$

where $\kappa^2 = 4R\rho/\{(R+\rho)^2 + (z-\zeta)^2\}$ is the argument of the complete elliptic integrals of the first kind K and the second kind E. For many coaxial current rings the flux function is given by linear superposition as $\psi(R,z) = \sum_i \Psi(R,z;\rho_i,\zeta_i)$. Hence the axisymmetric poloidal field is described as $B_R = -(1/R)\partial\psi/\partial z$ and $B_z = (1/R)\partial\psi/\partial R$. In the meanwhile the toroidal field is given by $B_\phi = B_\phi{}^o R_p/R$, where $B_\phi{}^o$ is the toroidal magnetic field at the major radius of the geometrical plasma center R_p.

Figure 1 shows the cross-sectional view of JT-60 with the coil arrangement. The plasma is assumed to be a filamentary ring located at the magnetic axis R_0. Therefore the magnetic surfaces are given correctly not far from the separatrix. The divertor configuration is generated mainly by the magnetic limiter coil ("ML-P" and "ML-S" in Fig. 1) current and the plasma current.

Typical parameters used in this paper is summarized in Table I. The equilibrium magnetic surfaces are illustrated in Fig. 2. Here the X point is located at R = 4.14 m on the equatorial plane, and q > 3 surfaces exist quite near the separatrix. The distance between q = 4 surface and the separatrix, for example, is about 10^{-4} m.

3. Effect of Toroidal Ripple Field

The toroidal ripple is generated due to the discrete nature of a toroidal coil system. Providing that the ripple field is dependent only on R and ϕ, the toroidal field is described by

$$B_\phi = B_\phi{}^0 R_p/R + B_{\phi 1}(R,\phi)$$
$$= B_{\phi 0}\{1 + \delta(R)\sin N\phi\} \quad ,$$

where δ is the ripple amplitude and N is the toroidal coil number. This assumption corresponds to the situation that the ripple field is produced by the straight and infinite N wires periodically located in z direction around the torus. With the aid of Maxwell's equations, we obtain $\delta = \delta_0 (R/R_p)^N$. Then the radial component of the ripple field is given by

$$B_R = -B_{\phi 0} \frac{\cos N\phi}{N} \frac{d\delta}{d(R/R_p)} \cdot$$

In JT-60 with N = 18 and R_p = 3 m, we have δ = 0.01 near the X point, corresponding to $\delta_0 = 3\times10^{-5}$. The distribution and the amplitude of the ripple field approximated in such a way agree well with the actual ones near the X point.[12]

Concerning the magnetic perturbations, of essential importance is the mode strength of the perturbation field perpendicular to a magnetic surface. Hence it is useful to expand the perpendicular perturbation in a Fourier series on the unperturbed flux surface ψ as following:

$$B_{\perp 1}(\psi,\theta,\phi) = \sum_{m,n} b_{mn}(\psi)\exp\{i(m\theta - n\phi)\},$$

where b_{mn} is the Fourier coefficient, m the poloidal mode number

and n the toroidal one, respectively. Figure 3 shows the mode strength b_{mn} of the toroidal ripple field acting on q = 4 surface. Since n = N = 18 in JT-60, the resonant mode strength on q = 4 surface is $b_{72,18}(\psi_{q=4}) = 6\times10^{-5}$ T. It is noted from Fig. 3 that the ripple field has the feature like a white noise with a small amplitude.

The field line equations including the toroidal ripple field are numerically integrated. The destruction of magnetic surfaces is examined by mapping the intersection points of a field line on a cross-sectional surface, and also by calculating the entropylike quantity of a field line.[13] The ergodic layer produced near the X point is illustrated in Fig. 4, which is attributed by the destruction of $q \gtrsim 4$ surfaces due to the overlapping of the island chains. Because the mode strength of the toroidal ripple field is small in JT-60, the ergodic layer is restricted within a narrow region with the width of about 5 mm, and bounds irregularly on the confined region. The strong shear effect prevents the ergodic layer from spreading in the divertor region.

4. Effect of Error Field due to Misalignment of Poloidal Coils

In any actual device there exists some displacement of coils from the ideal position, causing generation of non-axisymmetric field perturbations. Here we will consider the tolerances of a poloidal coil with the tilted and shifted position as shown in Fig. 5. If we employ local coordinates (R', ϕ', z') which are refered to the displaced coil, they are represented by the original coordinates as followings:

$$R' = [R^2\cos^2\phi+\{(R\sin\phi-\eta)\cos\alpha+z\sin\alpha\}^2]^{1/2}$$

$$\phi' = \tan^{-1}[\{(R\sin\phi-\eta)\cos\alpha+z\sin\alpha\}/R\cos\phi]$$

$$z' = -(R\sin\phi-\eta)\sin\alpha+z\cos\alpha$$

where α is the tilted angle and η is the shifted length. The field perturbation $B_1(B_{R1}, B_{\phi 1}, B_{Z1})$ induced by the coil displacement is given by

$$B_1 = SB_0' - B_0.$$

Here B_0 is the magnetic field without coil displacement, B_0' the magnetic field observed in the (R', ϕ', z') coordinates, and S the matrix associated with the coordinate transform:

$$S = \begin{pmatrix} \cos\phi & \sin\phi & 0 \\ -\sin\phi & \cos\phi & 0 \\ 0 & 0 & 1 \end{pmatrix} \begin{pmatrix} 1 & 0 & 0 \\ 0 & \cos\alpha & \sin\alpha \\ 0 & -\sin\alpha & \cos\alpha \end{pmatrix} \begin{pmatrix} \cos\phi' & -\sin\phi' & 0 \\ \sin\phi' & \cos\phi' & 0 \\ 0 & 0 & 1 \end{pmatrix}.$$

In JT-60, the misalignment of the magnetic limiter coils (ML-P and ML-S in Fig. 1) produces a large amount of the non-axisymmetric error field. The expected mechanical tolerance of this perturbation is summarized in Table II. Concerning the

toroidal mode number of the tilt perturbation or the shift one, the assumption of n = 1 is made for the present investigation.

Figure 6 shows the mode strength on q = 4 surface: (a) for the tilt perturbation of α = 3.5 mrad, and (b) for the shift perturbation of η = 8 mm. Here the resonant mode strength on q = 4 surface $b_{41}(\psi_{q=4})$ is indicated by the dark point for the respective cases. Since ML-S coil is located nearest to the separatrix in the plasma side, it produces a larger amount of the perturbed field than ML-P coil for both perturbations.

To understand the perturbed magnetic structure affected by the above perturbation with a low toroidal mode number (n=1), the following coil displacement is taken: (i) the tilt perturbation of ML-P coil, and (ii) perturbation composed of the tilt and shift perturbation of ML-P coil and ML-S coil. The essential feature of the perturbation is not changed in both cases, except the dependence of the mode strength b_{m1} on the poloidal mode number.

We will start with the investigation on the behavior of the field lines affected by the error field due to the tilt perturbation of ML-P coil with α = 3.5 mrad. The resonant mode strength on q = 3 surface and q = 4 surface is $b_{31}(\psi_{q=3}) = 4\times10^{-4}$ T and $b_{41}(\psi_{q=4}) = 5\times10^{-5}$ T, respectively.

For this case q = 3 magnetic islands are produced as plotted in Fig. 7. The width of the islands located far from the X point is 4.5 cm, which is almost consitent with the theoretical prediction:[14]

$$\Delta_{isl}^{(3)} = 4\{\frac{R_0}{n}\frac{b_{31}}{B_{\phi}{}^{0}}\frac{q}{dq/dr}|_{r=r_{q=3}}\}^{1/2} \quad .$$

The irregular behavior of the field lines is not clearly observed around the q = 3 island chain in this case.

On the other hand, $q \gtrsim 4$ surfaces are fully destroyed through the islands overlapping. The ergodic layer spreading near the X point is illustrated in Fig. 8 on the equatorial plane. The maximum width of the ergodic layer is about 3 cm. The outermost contour of q = 3 islands is located in the region of $R \lesssim 4.11$ m. As seen in Fig. 4 of the perturbed magnetic structure due to the toroidal ripple field, the ergodic layer near the X point penetrates the plasma side rather than the divertor side. The boundaries both between the ergodic layer and the confined region and between the ergodic layer and the divertor region fluctuate with n = 1 mode.

It is noted that the ergodic layer is composed of two kinds of region. The first kind of region is marked by a hatched area in Fig. 8 and is characterized by having a common toroidal circulation number N_C of the field lines until their flowing into the neutralizer plate. This circulation number is indicated in the respective hatched areas. It is noteworthy from Fig. 8 that most part of the ergodic layer is occupied by the region of the first kind with N_C of 11 or less. The second kind of region is represented by the narrow dotted area where various values of N_C lie scattered over a wide range of 4 to 100 or more. The similar property as the second kind of region appears dominantly in the ergodic layer produced by the toroidal ripple field.

At the same time, the ergodic layer spreading near the

separatrix in the innermost of the torus has the small width of about 3 mm. Again the first kind of region with N_C less than 10 is dominant in the whole ergodic layer. Figure 9 shows the path length of the field lines until reaching the neutralizer plate with and without the tilt perturbation, when the initial points are taken in the region of the torus: $2.23 \leq R < 2.25$, $\phi = 0$, and $z = 0$. The field line length in the first kind of the ergodic layer is about 100 m at $\phi = 0$ and 160 m at $\phi = \pi$, which is $3 \sim 5$ times longer than that in the divertor region.

In order to study the dependence of the magnetic island width as well as the ergodic layer width on the perturbation strength, the combined perturbation is introduced which is based on the tilt and shift perturbation of the magnetic limiter coils. For the case with the amplitude of $\alpha = 3.5$ mrad and $\eta = 8$ mm, the mode strength b_{m1} on $q = 3$ surface and $q = 4$ surface is plotted in Fig. 10 as a function of the poloidal mode number. The resonant mode strength on the respective surfaces is shown in Fig. 11 with the coefficient of the combined perturbation strength defined as $\gamma = \alpha/1.75$ [mrad] $= \eta/4$ [mm].

Figure 12 shows the dependence of the $q = 3$ island width $\Delta_{isl}^{(3)}$ on $b_{31}(\psi_{q=3})$. This island width is observed near the X point on the equatorial plane. Although $\Delta_{isl}^{(3)}$ at the above location does not mean the full width around the $q = 3$ island chain, the dependence of $\Delta_{isl}^{(3)}$ on $b_{31}(\psi_{q=3})$ is not changed. Figure 12 shows that $\Delta_{isl}^{(3)}$ scales with $\sqrt{b_{31}}$ if b_{31} is less than about 3×10^{-3} T ($\gamma \gtrsim 4 \sim 5$), and that after $\Delta_{isl}^{(3)}$ reaches its maximum size, the ergodic layer appears around $q = 3$ islands with a small width

$\Delta_{erg}^{(3)}$. It should be noted that the increase in $\Delta_{erg}^{(3)}$ consists with the decrease in $\Delta_{isl}^{(3)}$.

For the ergodic layer spreading near the separatrix due to the destruction of $q > 3$ surfaces, the first kind of region is dominant again in the entire area. The dependence of the ergodic layer width on $b_{41}(\psi_{q=4})$ is plotted in Fig. 13. Here $\Delta_{erg}^{(1)}$ means the ergodic layer width near the X point (as measured in Fig. 8), and $\Delta_{erg}^{(2)}$ in the innermost of the torus. As to $\Delta_{erg}^{(2)}$, Fig. 14 shows a typical example in case of $\gamma = 2$ [i.e. $b_{41}(\psi_{q=4}) = 2\times10^{-3}$ T]. The width $\Delta_{erg}^{(1)}$ connects continuously with $\Delta_{erg}^{(3)}$, as the perturbation increases its strength ($\gamma>4$). That is, the ergodic layer spreads near the X point with the width of $\Delta_{erg}^{(1)} + \Delta_{erg}^{(3)}$ and surrounds fully the $q = 3$ island chain.

One can find from Fig. 13 that $\Delta_{erg}^{(1)} + \Delta_{erg}^{(3)}$ is proportional to $\sqrt{b_{41}}$ and that $\Delta_{erg}^{(2)}$ increases linearly with b_{41}. This difference concerning the dependence on $b_{41}(\psi_{q=4})$ results from the distribution of the flux function itself in the divertor configuration near the separatrix. The width of the ergodic layer around the separatrix, Δ_{erg}, is generally estimated as $\Delta_{erg}^{(2)} < \Delta_{erg} < \Delta_{erg}^{(1)} + \Delta_{erg}^{(3)}$. Although the dependence agrees with the theoretical prediction,[7] the magnitude of Δ_{erg} is different from that based on the simple theory: $\Delta_{erg}^{(1)}/\Delta_{erg}^{(2)} \simeq 4$ at $b_{41}(\psi_{q=4}) = 2\times10^{-3}$ T in the present numerical calculation while $\Delta_{erg}^{(1)}/\Delta_{erg}^{(2)} \simeq 28$ in the theory. This is mainly because $\Delta_{erg}^{(2)}$ obtained numerically is by a factor of five wider than that predicted by the theory.

5. Discussions and Conclusions

In the absence of the non-axisymmetric magnetic perturbations, the scrape-off layer width Δ_{scr} predicted by the emperical scaling law of DIVA[15] is $1 \sim 2$ cm over a wide range of expected plasma parameters in JT-60, while the clearance between the separatrix and the nearest first wall is $3 \sim 4$ cm for $\beta_p=1$ and $\ell_i=1$. Once the ergodic layer is formed near the separatrix, however, the clearance generally becomes narrow. Some part of the field lines in the scrape-off layer may strike the first wall before their reaching the neutralizer plate, if $\Delta_{scr}+\Delta_{erg}^{(2)}$ is wider than the clearance. To avoid this situation, $\Delta_{erg}^{(2)}$ must be kept smaller than Δ_{scr}.

From this point of view, the width of the ergodic layer has been estimated in §3 and §4. The toroidal ripple field produces the ergodic layer with the narrow width: $\Delta_{erg}^{(1)} = 0.5$ cm for the ripple amplitude of JT-60. In the meanwhile, the error field due to the misalignments of the magnetic limiter coils have a possibility to produce the ergodic layer with a wide width. We have considered the coil perturbations with n=1 mode, because it is the most dangerous case that destroys the magnetic surfaces near the separatrix. From the engineering viewpoint of the coil installation in JT-60, the mechanical tolerance of the magnetic limiter coils is expected to be kept less than $\gamma=1$[16]: $b_{31}(\psi_{q=3}) \lesssim 6\times10^{-4}$ T and $b_{41}(\psi_{q=4}) \lesssim 1\times10^{-3}$ T. At this level of mechanical tolerance, the ergodic layer is localized with $\Delta_{erg}^{(1)} = 4$ cm near the X point and $\Delta_{erg}^{(2)} = 0.6$ cm in the innermost of the torus as shown in Fig. 13. Thus the relation of $\Delta_{erg}^{(2)} < \Delta_{scr}$ will be satisfied in JT-60. Moreover if the misalignments occur at

a few locations (i.e. n > 1), it will be possible to reduce the resonant mode strength and consequently the ergodic layer width.

Concerning the possibility of particle loss mechanism, it is found from Figs. 8 and 9 that most of the field lines in the first kind of the ergodic layer flow into the neutralizer plate with the path length of 100 ∿ 200 m. This path length corresponds to the mean free path of electrons at the boundary plasma with $n_e = (0.5 \sim 1.0) \times 10^{19}$ m^{-3} and $T_e = 200 \sim 300$ eV. Therefore without collisions these epithermal electrons will escape from the boundary region. But it is not clear whether or not these electrons directly strike the neutralizer plate, because the present calculation is based on a vacuum magnetic field system. As to the possibility of the heat flux reduction on the neutralizer plate induced by the ergodicity of the field lines, we did not obtain the manifest result. Namely, it is not obviously observed in the present investigation that the field lines leaking from the ergodic layer in the plasma side sufficiently spread on the neutralizer plate within one poloidal circuit. Then a more precise calculation, including particle motions in a scrape-off layer plasma as well as in a perturbed magnetic field, is required further to understand the particle and heat flow onto the neutralizer plate in JT-60.

Finally we conclude by summarizing main results obtained in the present investigations as follows:

(1) Toroidal ripple field produces the ergodic layer with a narrow width due to its non-resonant nature with a high toroidal mode number: $\Delta_{erg}^{(1)} = 0.5$ cm even near the X point for the ripple amplitude of 0.01.

(2) Error field with a low toroidal mode number can produce the ergodic layer with a wide width: $\Delta_{erg}^{(1)}$ = 4 cm near the X point and $\Delta_{erg}^{(2)}$ = 0.6 cm in the innermost of the torus for the presumed mechanical tolerance of the magnetic limiter coils.

(3) Particle loss will be enhanced at the boundary plasma, particularly when magnetic perturbation has a low toroidal mode number (n=1) and a wide profile of a poloidal mode number with a peak at m∿nq as shown in Figs. 6 and 10.

Acknowledgements

The authors are grateful to Drs. Y. Shimomura and S. Seki for their useful discussions. Drs. M. Yoshikawa and M. Tanaka are gratefully acknowledged for their continuous encouragement.

(2) Error field with a low toroidal mode number can produce the ergodic layer with a wide width: $\Delta_{erg}^{(1)}$ = 4 cm near the X point and $\Delta_{erg}^{(2)}$ = 0.6 cm in the innermost of the torus for the presumed mechanical tolerance of the magnetic limiter coils.

(3) Particle loss will be enhanced at the boundary plasma, particularly when magnetic perturbation has a low toroidal mode number (n=1) and a wide profile of a poloidal mode number with a peak at m∿nq as shown in Figs. 6 and 10.

Acknowledgements

The authors are grateful to Drs. Y. Shimomura and S. Seki for their useful discussions. Drs. M. Yoshikawa and M. Tanaka are gratefully acknowledged for their continuous encouragement.

References

1) Y. Shimomura and H. Maeda: J. Nucl. Mater. 76 & 77 (1978) 45.

2) M.N. Rosenbluth, R.Z. Sagdeev, J.B. Taylor and G.M. Zaslavski: Nucl. Fusion 6 (1966) 297.

3) G.M. Filonenko, R.Z. Sagdeev and G.M. Zaslavski: Nucl. Fusion 7 (1967) 253.

4) F.M. Hamzeh: Nucl. Fusion 14 (1974) 523.

5) A.B. Rechester and M.N. Rosenbluth: Phys. Rev. Lett. 40 (1978) 38.

6) S. Yamamoto, S. Sengoku, H. Kimura, Y. Shimomura, H. Maeda, H. Ohtsuka, K. Odajima, M. Nagami, N. Ueda: Nucl. Fusion 18 (1978) 205.

7) Y. Tomita, S. Seki and H. Momota: J. Phys. Soc. Japan 44 (1978) 637.

8) A.H. Boozer and A.B. Rechester: Phys. Fluids 21 (1978) 682.

9) D.I. Brown: Princeton Plasma Physics Loboratory Report PPPL-1433 (1978).

10) A.V. Bazaeva, V.E. Bykov, A.V. Georgievskij, I.N. Golovin, A.O. Kaminskij, L.V. Mikhajlovskaya, V.G. Peletminskaya, V.N. Pyatov: Nucl. Fusion 20 (1980) 83.

11) D.L. Jassby (compiler): Nuclear Fusion 17 (1977) 373, and B.J. Green (compiler): Nuclear Fusion 19 (1979) 515.

12) S. Nishio, M. Ohkubo, K. Kawasaki, T. Ando and N. Miki: JAERI-M 7846 (1978) [in Japanese].

13) Detailed results of this computation will be published elsewhere.

14) S. Matsuda and M. Yoshikawa: Japan J. Appl. Phys. 14 (1975)

87.

15) DIVA Group: Nucl. Fusion 18 (1978) 1619.

16) T. ANDO: private communication.

Table I Typical parameters for calculations of plasma equilibrium and field line equations

Poloidal beta	$\beta_p = 1$	
Internal inductance	$\ell_i = 1$	
Magnetic axis	$R_0 = 3.2$	[m]
Toroidal field	$B_\phi{}^\circ = 4.5$	[T]
Plasma current	$I_p = 2.1$	[MA]
Primary magnetic limiter (ML-P) coil current	$I_{ML-P} = 90$	[kA/turn]
Sub magnetic limiter (ML-S) coil current	$I_{ML-S} = -90$	[kA/turn]
Vertical field coil current	$I_V = 34$	[kA/turn]
Quadrupole field coil current	$I_Q = 17$	[kA/turn]
Horizontal field coil current	$I_H = 0$	

Table II Typical examples of magnetic perturbations

Origins	Amplitude	Location(Toroidal mode number)
Toroidal ripple field	δ=0.01	Near X point (n=18)
Tilt perturbation	α=1.75 mrad	Magnetic limiter coils (n=1)
Shift perturbation	η= 4 mm	Magnetic limiter coils (n=1)

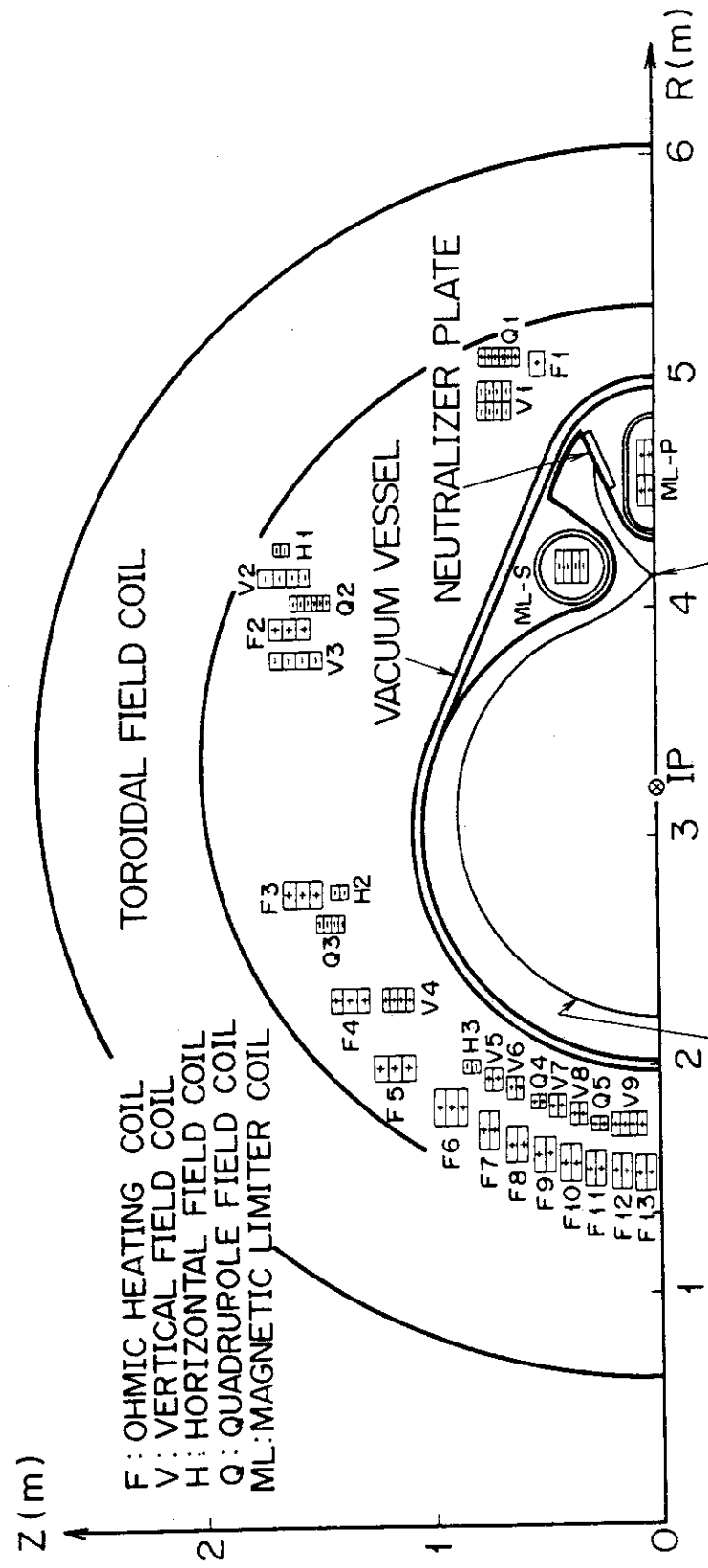

Fig. 1 Cross-sectional view of JT-60. The positions of poloidal field coils used in this calculation are illustrated.

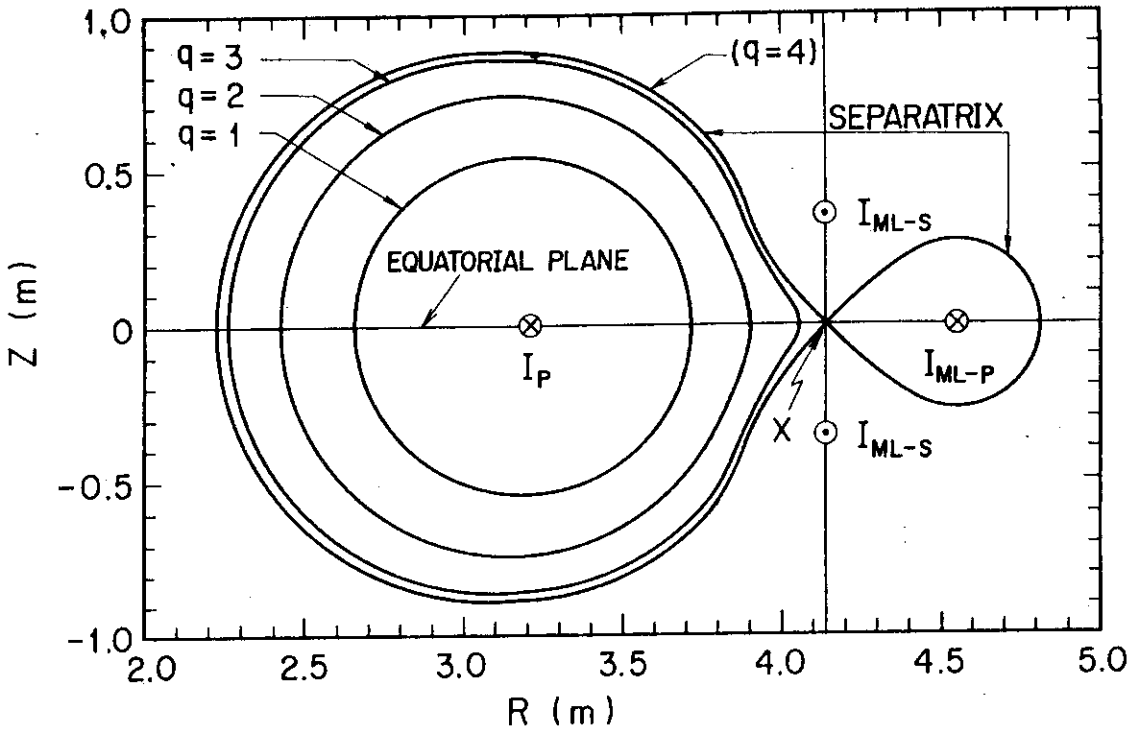

Fig. 2 Axisymmetric magnetic configuration. The X point is marked by "X".

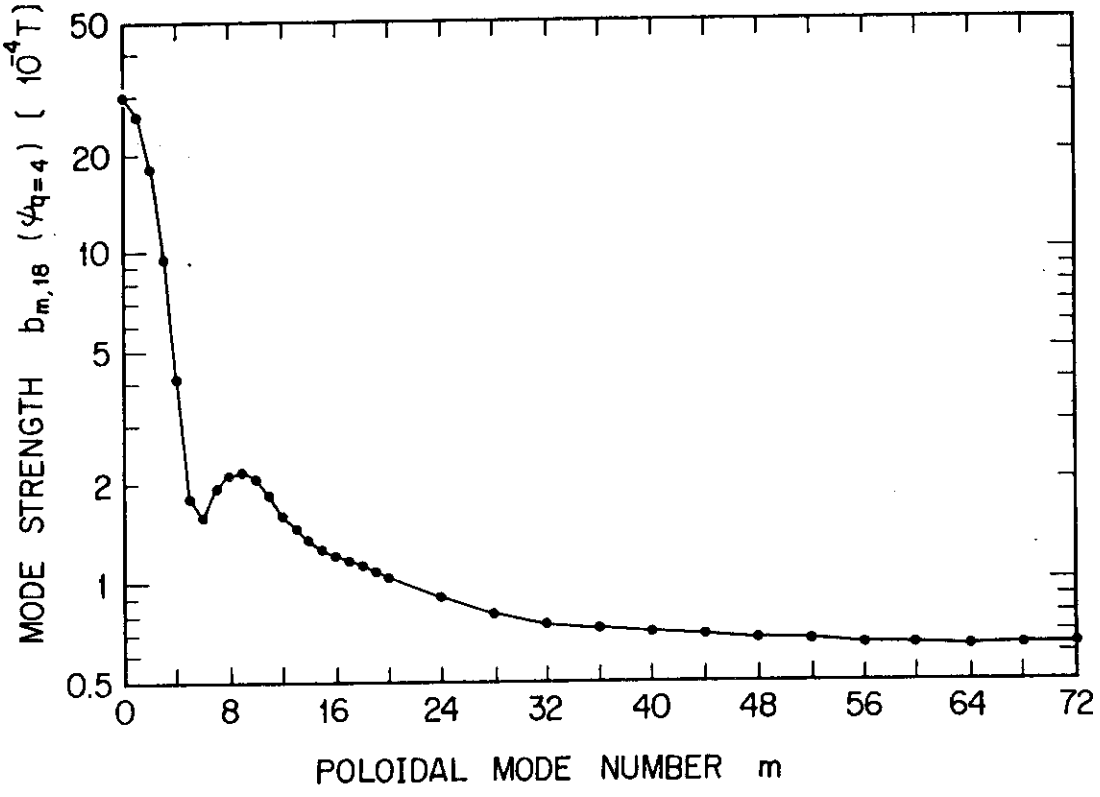

Fig. 3 Mode strength of toroidal ripple field perpendicularly acting on q=4 surface with poloidal mode number.

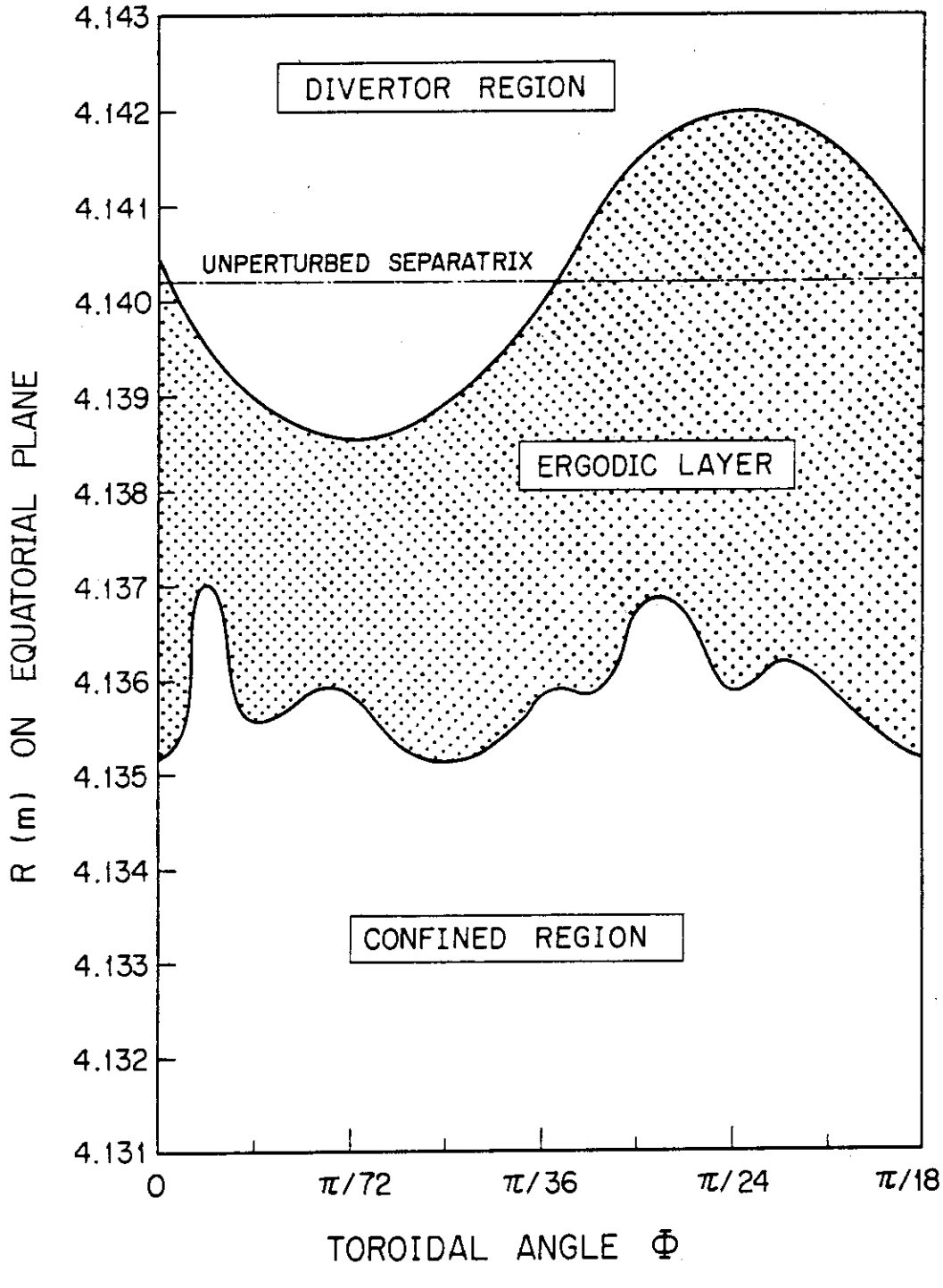

Fig. 4 Perturbed magnetic structure near the X point on equatorial plane affected by toroidal ripple field. The ergodic layer bounds irregularly on the confined region.

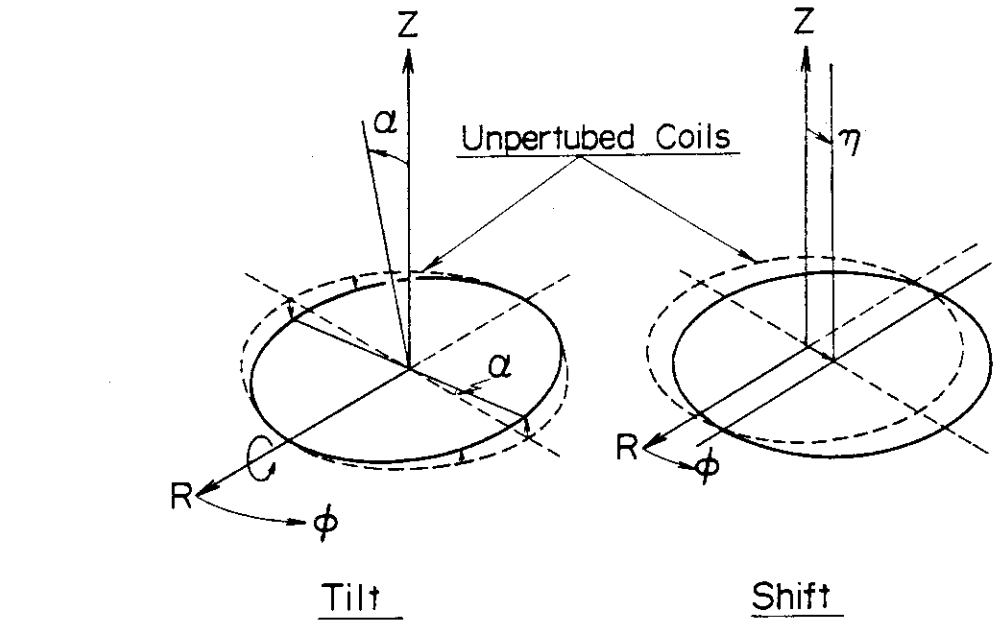

Fig. 5 Illustration of tilt and shift displacements of poloidal coil.

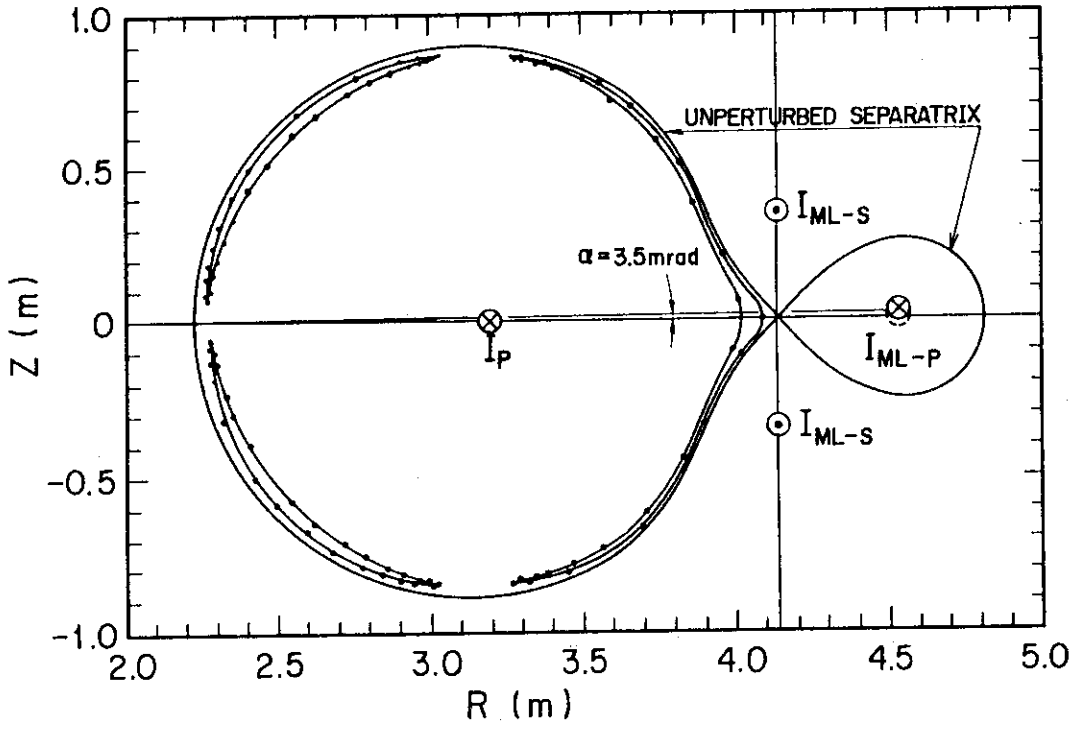

Fig. 7 q=3 magnetic islands produced by error field due to 3.5 mrad tilted ML-P coil.

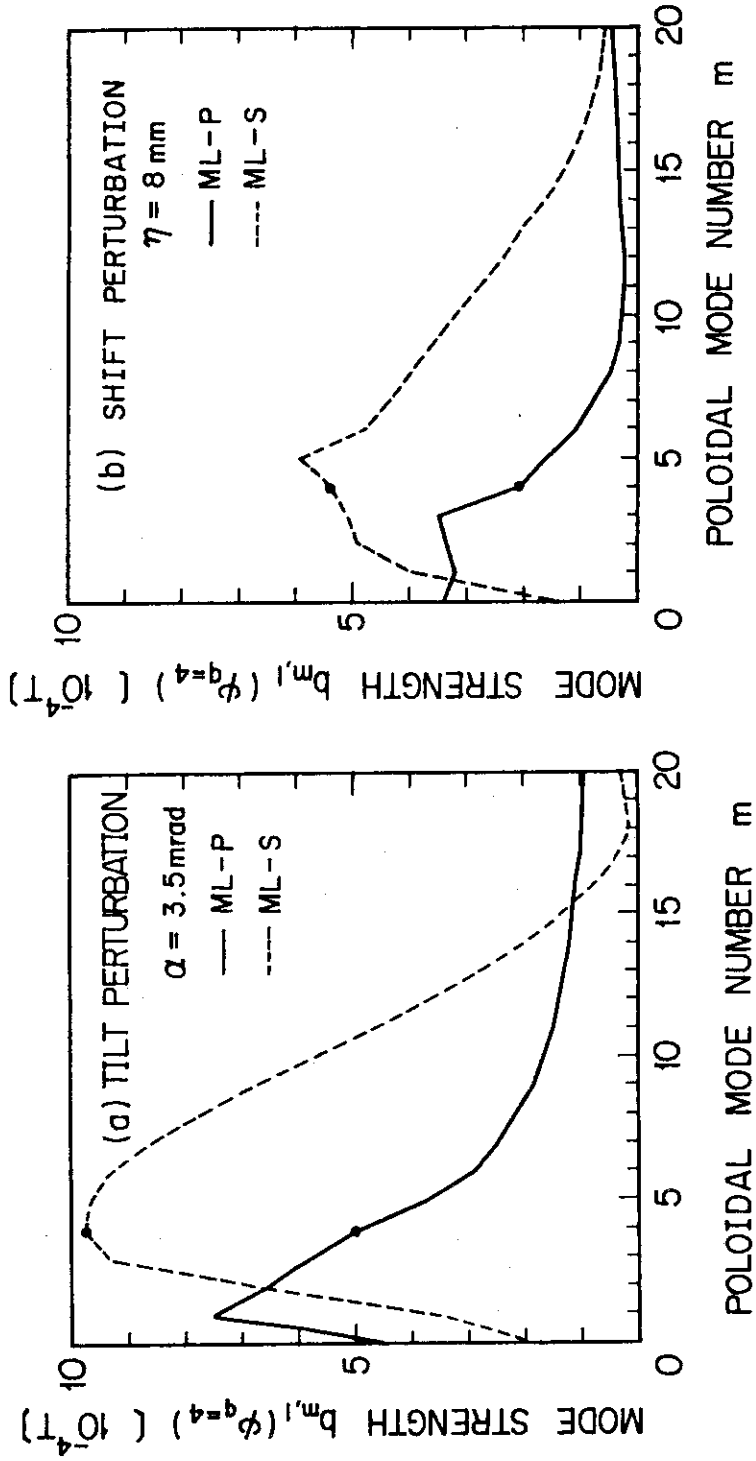

Fig. 6 Mode strength of error field due to coil displacement of magnetic limiter:
(a) tilt perturbation of α=3.5 mrad,
(b) shift perturbation of η=8 mm.
The dark point shows the resonant mode strength on q=4 surface.

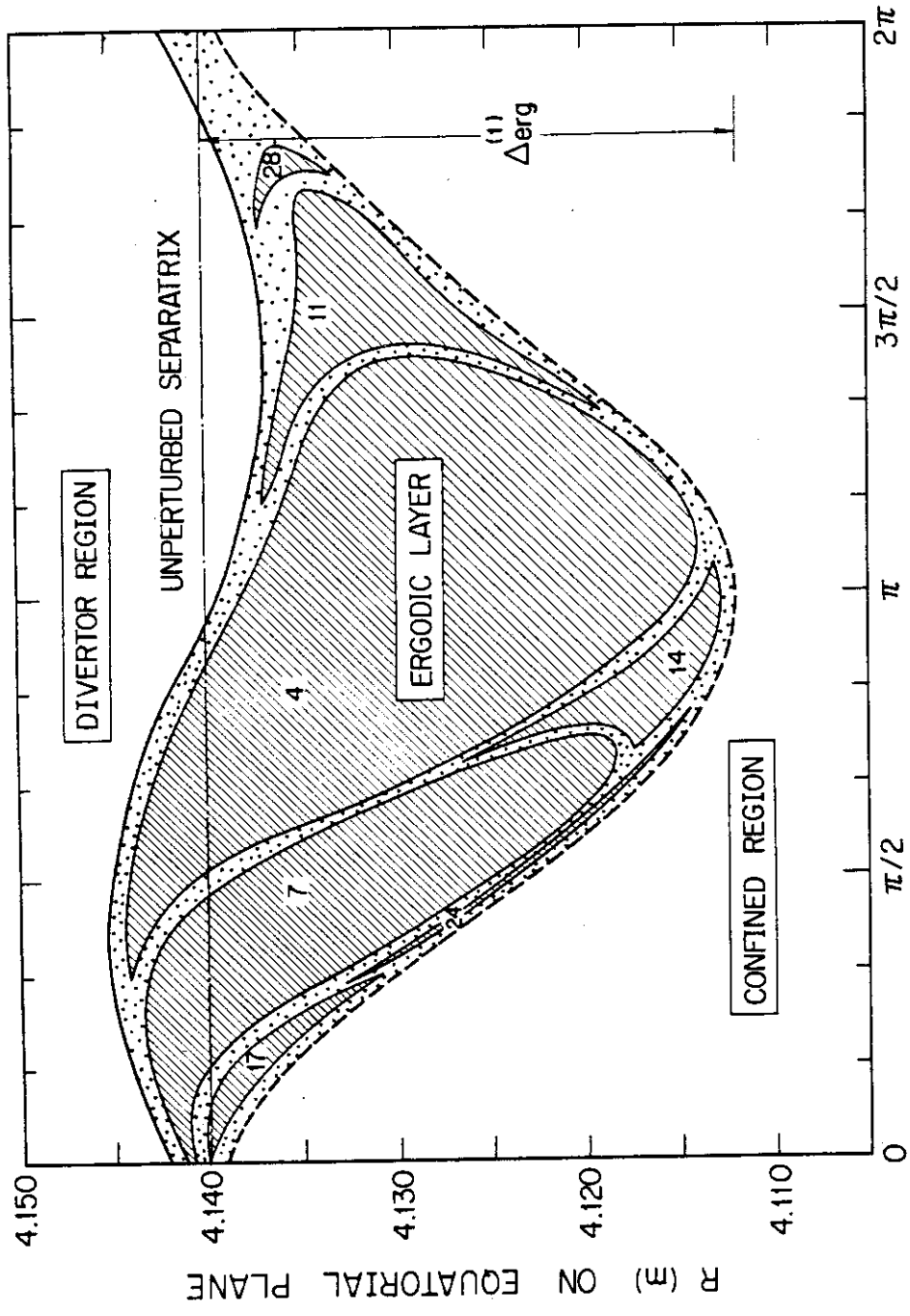

Fig. 8 Ergodic layer produced by error field due to 3.5 mrad tilted ML-P coil. Number in each hatched area means the circulations of field lines around the torus until following out.

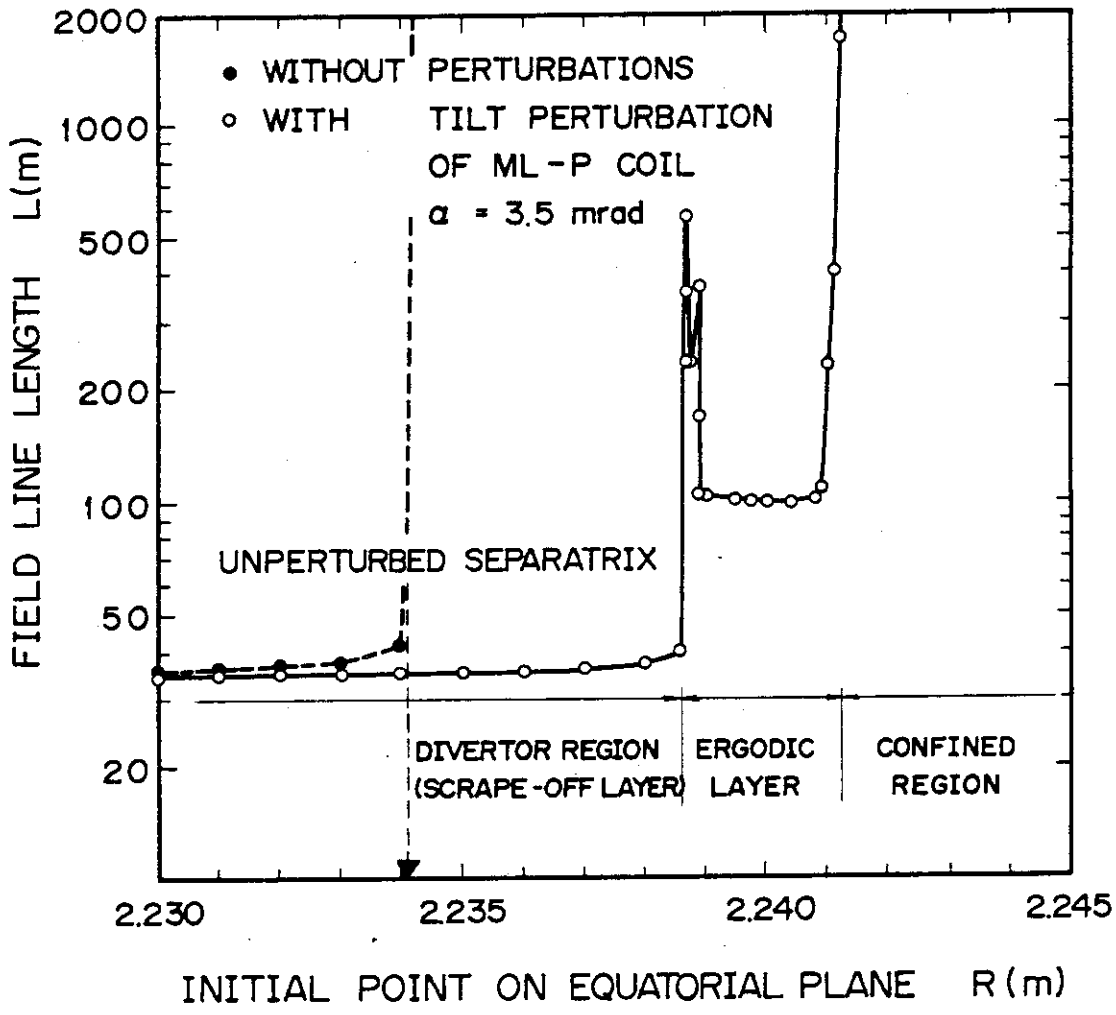

Fig. 9 Field line length until reaching the neutralizer plate with initial point at $\phi=0$ on equatorial plane. Solid line shows field line length with tilt perturbation of 3.5 mrad for ML-P coil, while dotted line without perturbation for reference.

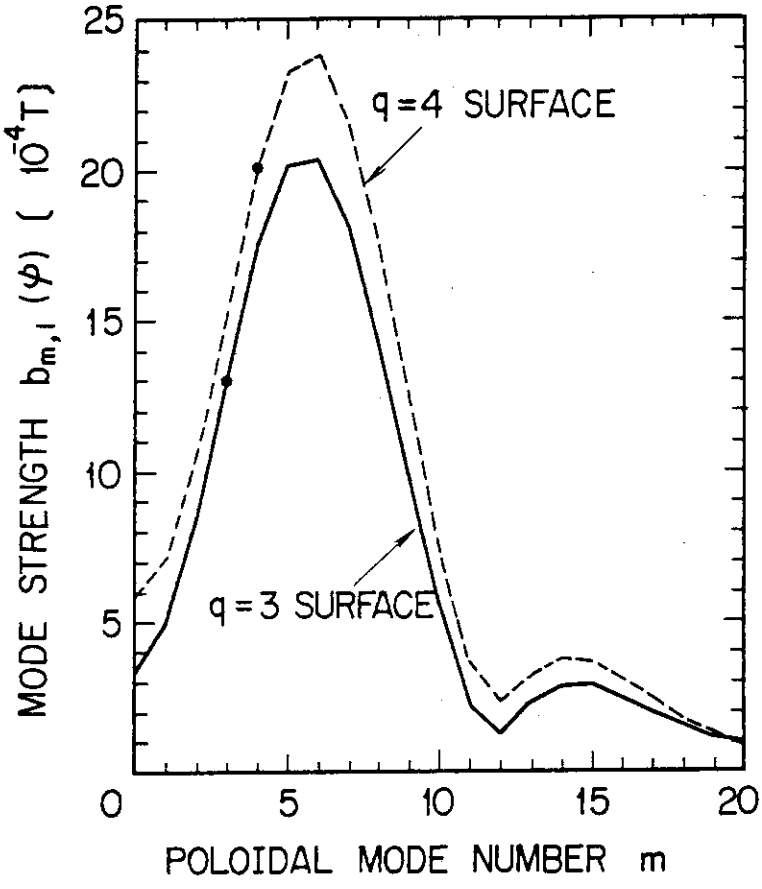

Fig.10 Mode strength of combined perturbation on q=3 surface and on q=4 surface. Combined perturbation, in this case, is based on the tilt and shift perturbation of magnetic limiter coils with α=3.5 mrad and η=8 mm, respectively. The dark point shows the resonant mode strength.

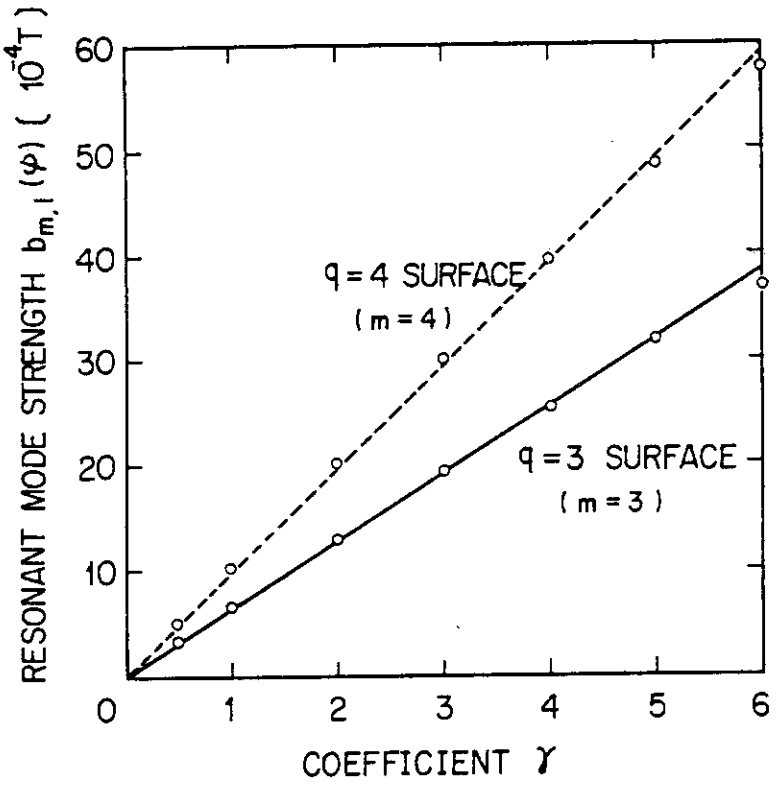

Fig.11 Resonant mode strength on q=3 surface and q=4 surface with the coefficient of combined perturbation strength defined as $\gamma = \alpha/1.75$ [mrad] $= \eta/4$ [mm].

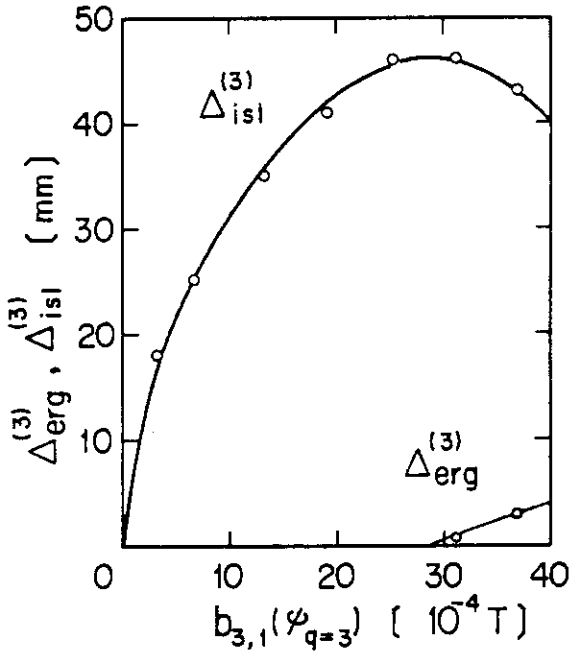

Fig.12 q=3 island width $\Delta^{(3)}_{isl}$ and ergodic layer width around it $\Delta^{(3)}_{erg}$ observed at $\phi = \pi/3$ on equatorial plane near the X point as a function of the resonant mode strength on q=3 surface.

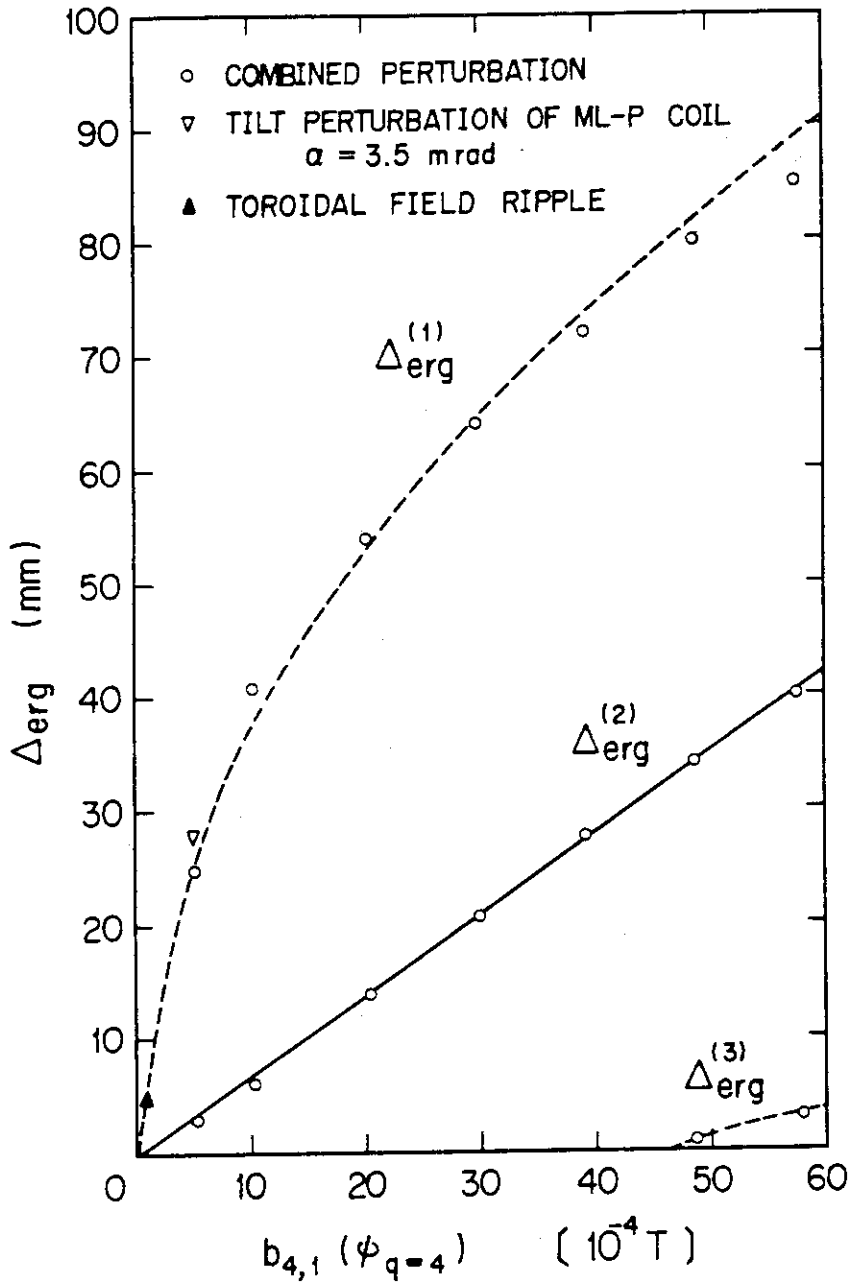

Fig.13 The dependence of ergodic layer width produced by combined perturbation on the resonant mode strength on q=4 surface. $\Delta_{erg}^{(1)}$ means the ergodic layer width near the X point, $\Delta_{erg}^{(2)}$ in the opposite side of the X point, and $\Delta_{erg}^{(3)}$ around q=3 island. $\Delta_{erg}^{(1)}$ produced by toroidal ripple field and by 3.5 mrad tilted ML-P coil are also plotted, respectively.

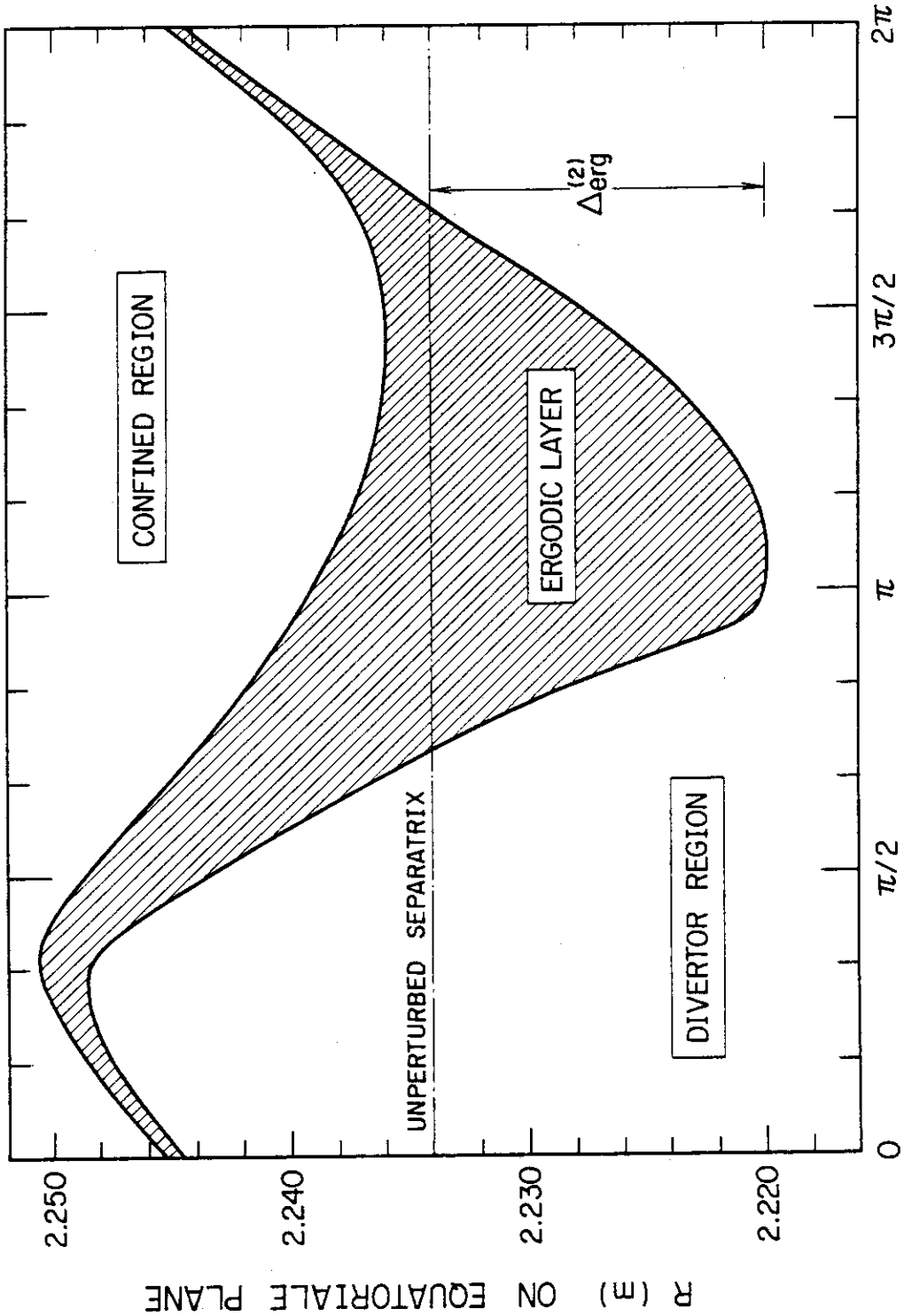

Fig.14 Ergodic layer observed in the innermost of the torus under the influence of combined perturbation (γ=2).